J. Fluid Mech. (1973), *vol.* 58, *part* 4, *pp.* 641–656
Printed in Great Britain

Low-Reynolds-number fall of slender cylinders near boundaries

By N. J. DE MESTRE

Department of Mathematics, Royal Military College,
Duntroon, Australia

(Received 20 September 1972 and in revised form 26 January 1973)

The motion of bodies through fluid at low Reynolds number is appreciably affected by the container walls. Consequently the Stokes-flow theory due to Batchelor (1970) and others for a slender body falling in an unbounded fluid is difficult to test experimentally unless it is extended to take account of nearby boundaries. Theoretical expressions are given here for certain drag coefficients of a circular cylindrical slender rod of finite length falling *close* to a single plane wall or falling midway between two parallel plane walls. Experiments with a very viscous liquid are described in which cylinders of small thickness-to-length ratios (ranging from 1:10 to 1:100 approximately) are made to fall in suitable orientations. From their times of fall over a measured distance experimental drag coefficients are determined and compared with the corresponding theoretical value from the extension of Batchelor's theory. For rods falling in a horizontal orientation the theoretical and experimental results are consistent within the order of accuracy of the experiments. However, when results are compared for rods falling in a vertical orientation there is a significant difference for which possible explanations are presented.

1. Introduction

The recent interest in slender-body Stokes-flow theory expressed by Taylor (1969), Batchelor (1970), Cox (1970, 1971), Tillett (1970), Clarke (1972) and Weinberger (1972) has created a need for a comparison between the predictions of this theory and some corresponding experimental results.

It appears that direct testing of the theory for a slender body falling in an unbounded fluid is difficult, because the length of the slender body would have to be simultaneously large compared with its thickness and small compared with the distance from the centre of the body to the nearest wall of the container.

Only a few experiments seem to have been previously reported (White 1946; Jones & Knudsen 1961). Recently Dr S. Thompson communicated to me the results of his slender-body experiments carried out at the Ministry of Works, Wellington, New Zealand. Although each of these experimenters referred to the influence of the dimensions of the containing vessel on the drag coefficient of long slender cylinders in the creeping-motion range, the lack of well-established wall-correction factors has prevented any useful comparison between theory and experiment.

This suggests that a more detailed analysis of the wall effects on a falling slender body is worthwhile. From the ensuing theory it can be deduced that it is not possible for a rod falling near a plane wall (or between two plane walls) to maintain a particular orientation except in a few special situations. This has been confirmed by experimental observation and consequently the present paper produces appropriate Stokes-flow expressions for the drag coefficient of a circular cylinder falling in (i) a horizontal orientation near a single plane wall, (ii) a horizontal orientation midway between two parallel plane walls and (iii) a vertical orientation midway between two parallel plane walls. In each of these problems the axis of the cylinder is parallel to a wall, and the orientation remains steady during the fall. (The wall-effect analysis may prove useful in its own right; a recent paper by Blake (1971) points to the use of slender-body theory for a body near a wall in modelling the movement of micro-organisms in the vicinity of microscope slides.)

The mathematical analysis extends the work of Batchelor (1970) and is based on the use of point force singularities, usually referred to as Stokeslets, to replace the effect of the finite cylindrical rod. Expressions which include the drag effects of these walls are derived with the aid of a mirror-image technique due to Lorentz (1896) for (i) and an extension of the technique due to Faxen (1923) for (ii) and (iii).

Suitable experiments associated with the above three problems have been performed. These involve a rectangular tank filled with liquid glucose in which metal rods of various small thickness-to-length ratios are induced to fall. Each rod moves with its axis parallel to a long wall and such that its centre is equidistant from both short walls, the latter being a large distance apart to reduce their effect on the drag. In these experiments the terminal speed of a rod is measured, followed by the terminal speed of a tiny standard sphere to ascertain the liquid's viscosity. Certain basic measurements of the rod and the standard sphere are then combined with these speeds to yield experimental drag coefficients for comparison with the values from the slender-body, wall-corrected mathematical analysis.

2. Slender-body theory including wall effects

Suppose a rigid rod in the shape of a long thin circular cylinder of length $2l$ and radius R_0 is falling through a viscous fluid. The rod is considered to be a slender body if its length is large compared with its diameter, and it is convenient to define a thickness-to-length parameter

$$\epsilon = \{\ln (2l/R_0)\}^{-1},$$

which is small for slender bodies.

The viscous fluid is disturbed as the rod falls, and in slender-body theory the associated flow field at low Reynolds number is investigated by looking at an almost equivalent problem in which the falling rod is replaced by a line distribution of Stokeslets of unknown strengths along the axis of the cylinder. For a rod falling longitudinally or transversely in unbounded fluid Batchelor (1970)

obtained approximate expressions for these unknown strengths by employing the no-slip condition on the curved boundary of the rod. If walls are present as boundaries of the fluid it is expected that these expressions for the unknown Stokeslet strengths will be modified.

Undoubtedly the simplest boundary geometry to consider is that of a plane wall. However, analysis and experiment indicate, as will be shown, that a rod falling in a vertical orientation parallel to a single plane wall cannot maintain this particular orientation. Therefore the wall effects for a rod falling midway between two parallel vertical walls are also considered since the vertical orientation is preserved in this case.

The method used in this paper to obtain the wall-correction factor for the drag on a rod falling through a viscous fluid in the presence of a single wall is essentially a mirror-image technique. When this method is applied to the double-wall situation it gives a wall-correction factor in the form of a series that is of little practical use. The double-wall situation is investigated more profitably by an adaptation of Faxen's (1923) technique for a sphere falling between two parallel walls. Hence the single-wall and double-wall situations are considered separately.

In the application of both techniques it is convenient to choose a set of axes that are fixed with respect to the moving rod. It then follows that, when the no-slip condition is satisfied on both the rod and the walls, the perturbation velocity due to the line distribution of Stokeslets is equal to the velocity of the rod at all points of the rod's surface and is zero everywhere on the walls.

2.1. *Horizontal orientation, single plane wall*

For a rod in a horizontal orientation moving transversely with velocity U_1 parallel to a fixed vertical plane wall, a rectangular set of co-ordinate axes is chosen to move with the rod. The origin is at the centre of the rod, the x axis is parallel to the rod, the y axis points in the direction of the rod's motion, and the z axis is perpendicular to the wall (see figure 1). If the rod is a distance L from the wall, the equation of the wall's surface is $z = L$.

Suppose a line distribution of Stokeslets with strengths $(0, F_1(x), 0)$ covers the portion $-l < x < +l, y = 0, z = 0$ of the cylinder's axis; then for flows in which inertia forces are neglected the approach employed by Batchelor (1970) formulates the perturbation velocity components (u_0, v_0, w_0) and the pressure p_0 at any point (x, y, z) for an unbounded fluid as

$$u_0(x,y,z) = \frac{1}{8\pi\mu}\int_{-l}^{+l} \frac{y(x-x')\,F_1(x')}{r_0^3}\,dx',$$

$$v_0(x,y,z) = \frac{1}{8\pi\mu}\int_{-l}^{+l} \left(\frac{1}{r_0}+\frac{y^2}{r_0^3}\right) F_1(x')\,dx',$$

$$w_0(x,y,z) = \frac{1}{8\pi\mu}\int_{-l}^{+l} \frac{yzF_1(x')}{r_0^3}\,dx',$$

$$p_0(x,y,z) = \frac{1}{4\pi}\int_{-l}^{+l} \frac{yF_1(x')}{r_0^3}\,dx' + \text{constant},$$

where $r_0^2 = (x-x')^2 + y^2 + z^2$ and μ denotes the dynamic viscosity of the fluid.

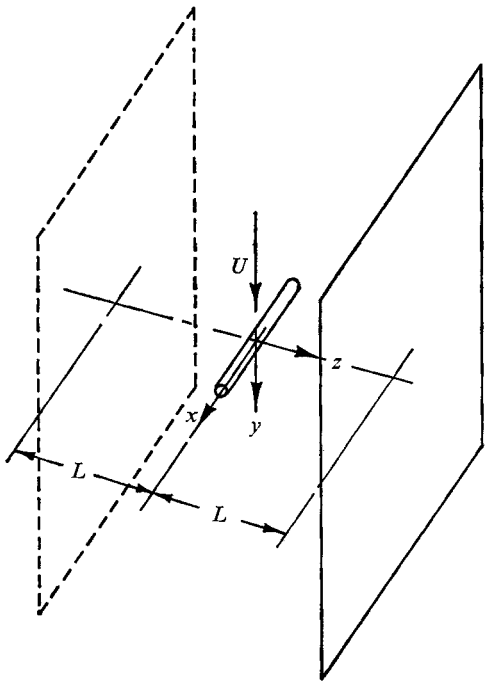

FIGURE 1. Cylindrical rod with a horizontal orientation falling parallel to a single plane vertical wall ($z = L$) or midway between the two parallel walls ($z = \pm L$).

To satisfy the no-slip condition on the wall, a new solution (u_1, v_1, w_1) of the creeping-motion equations is added to the solution (u_0, v_0, w_0) such that $u_1 = -u_0$, $v_1 = -v_0$ and $w_1 = -w_0$ when $z = L$. This new solution is obtained by using a distribution of image point forces with the same strengths as before along the line segment $-l < x < +l$, $y = 0$, $z = 2L$. These yield a solution $(u_2, v_2, w_2; p_2)$ similar to the solution $(u_0, v_0, w_0; p_0)$ except that $z - 2L$ replaces z, and then the required solution (u_1, v_1, w_1) is produced by the formulae (see Happel & Brenner 1965, p. 87):

$$(u_1, v_1, w_1) = (-u_2, -v_2, w_2) - 2(z-L)\left(\frac{\partial}{\partial x}, \frac{\partial}{\partial y}, \frac{\partial}{\partial z}\right) w_2 + \frac{(z-L)^2}{\mu}\left(\frac{\partial}{\partial x}, \frac{\partial}{\partial y}, \frac{\partial}{\partial z}\right) p_2.$$

Thus, within the accuracy afforded by replacing a rod by a line distribution of Stokeslets, the perturbation velocity components (u, v, w) at any point (x, y, z) of a viscous fluid in which a rod is falling in a horizontal orientation parallel to and distance L from a vertical plane wall are given by

$$u = u_0 + \frac{1}{8\pi\mu}\int_{-l}^{+l}\left\{-\frac{y(x-x')}{r_2^3} - \frac{6Ly(x-x')(z-L)}{r_2^5}\right\} F_1(x')\,dx', \tag{2.1}$$

$$v = v_0 + \frac{1}{8\pi\mu}\int_{-l}^{+l}\left\{-\frac{1}{r_2} + \frac{2L(z-L)-y^2}{r_2^3} - \frac{6Ly^2(z-L)}{r_2^5}\right\} F_1(x')\,dx', \tag{2.2}$$

$$w = w_0 + \frac{1}{8\pi\mu}\int_{-l}^{+l}\left\{-\frac{yz}{r_2^3} - \frac{6Ly(z-2L)(z-L)}{r_2^5}\right\} F_1(x')\,dx', \tag{2.3}$$

where $r_2^2 = (x-x')^2 + y^2 + (z-2L)^2$.

The unknown strengths F_1 are now determined from the boundary condition that (u, v, w) equals $(0, U_1, 0)$ everywhere on the rod's surface. Strictly, the no-slip condition should allow for a rotation of the rod about its own axis caused by its proximity to the wall. It can be shown that the inclusion of this rotation effect does not alter the leading terms of the slender-body expansion for the Stokeslet strengths, therefore the simpler no-slip condition is considered here. This leads to three integral equations for F_1, thus making provision for the introduction of higher-order Stokeslet singularities or even potential flow singularities if they are desired (Tuck 1964, 1968; Taylor 1969; Tillett 1970). However, as pointed out by Batchelor (1970), the total force exerted by the rod on the fluid is determined by the Stokeslet distribution alone, and so it suffices in slender-body theory to derive F_1 from the condition that $v = U_1$ at all points (x_s, y_s, z_s) of the rod's curved surface $(R_0 = (y_s^2+z_s^2)^{\frac{1}{2}},\ -l \leqslant x_s \leqslant +l)$. It will be indicated at the end of this section how the neglected conditions $(u = 0, w = 0)$ can be used.

Hence from (2.2),

$$\begin{aligned}
8\pi\mu U_1 = {} & F_1(x_s)\int_{-l}^{+l}\left(\frac{1}{r_{0s}}+\frac{y^2}{r_{0s}^3}\right)dx' \\
& + F_1(x_s)\int_{-l}^{+l}\left\{-\frac{1}{r_{2s}}+\frac{2L(z_s-L)-y_s^2}{r_{2s}^3}-\frac{6Ly_s^2(z_s-L)}{r_{2s}^5}\right\}dx' \\
& + \int_{-l}^{+l}\left(\frac{1}{r_{0s}}+\frac{y_s^2}{r_{0s}^3}\right)\{F_1(x')-F_1(x_s)\}\,dx' \\
& + \int_{-l}^{+l}\left\{-\frac{1}{r_{2s}}+\frac{2L(z_s-L)-y_s^2}{r_{2s}^3}-\frac{6Ly_s^2(z_s-L)}{r_{2s}^5}\right\}\{F_1(x')-F_1(x_s)\}\,dx' \\
\equiv {} & I_1+I_2+I_3+I_4.
\end{aligned}$$

This integral equation is solved approximately for F_1 by invoking slender-body approximations. It is convenient at this stage to drop the s subscript, and with $y = R_0\cos\theta$ and $z = R_0\sin\theta$ it is seen that, as $R_0/l \to 0$ and $R_0/L \to 0$,

$$I_1 = F_1(x)\left[2\ln\frac{2l}{R_0}+\ln\left(1-\frac{x^2}{l^2}\right)+2\cos^2\theta+O\left(\frac{R_0^2}{l^2}\right)\right],$$

$$\begin{aligned}
I_2 = F_1(x)\Bigg[& -\operatorname{arcsinh}\left(\frac{l+x}{2L}\right)-\operatorname{arcsinh}\left(\frac{l-x}{2L}\right)-\frac{l+x}{2\{(l+x)^2+4L^2\}^{\frac{1}{2}}} \\
& -\frac{l-x}{2\{(l-x)^2+4L^2\}^{\frac{1}{2}}}+O\left(\frac{R_0}{L}\right)+O\left(\frac{R_0}{l}\right)\Bigg],
\end{aligned}$$

$$I_3 = \int_{-l}^{+l}\frac{F_1(x')-F_1(x)}{|x'-x|}\,dx'+O\left[\frac{\{F_2(x')-F_2(x)\}R_0^2}{l^2}\right],$$

$$\begin{aligned}
I_4 = {} & -\int_{-l}^{+l}\frac{F_1(x')-F_1(x)}{\{(x-x')^2+4L^2\}^{\frac{1}{2}}}\,dx'-2L^2\int_{-l}^{+l}\frac{F_1(x')-F_1(x)}{\{(x-x')^2+4L^2\}^{\frac{3}{2}}}\,dx' \\
& +O\left[\frac{\{F_1(x')-F_1(x)\}R_0L}{l^2}\right]+O\left[\frac{\{F_1(x')-F_1(x)\}R_0l}{L^2}\right].
\end{aligned}$$

In the spirit of Batchelor's approach, the troublesome term in the expansion of I_1 which contains the azimuthal angle θ is removed by considering an 'inner'

flow field solution in the neighbourhood of the rod. When this is obtained and the appropriate matching is carried out, the integral equation for F_1 becomes

$$4\pi\mu U_1 = F_1(x)\left[\frac{1}{\epsilon}+\tfrac{1}{2}\ln\left(1-\frac{x^2}{l^2}\right)+\tfrac{1}{2}-E_1(x)+O\left(\frac{R_0}{L}\right)+O\left(\frac{R_0}{l}\right)\right]$$
$$+\frac{1}{2}\int_{-l}^{+l}\left[\frac{1}{|x'-x|}-\frac{(x-x')^2+6L^2}{\{(x-x')^2+4L^2\}^{\frac{3}{2}}}\right]\{F_1(x')-F_1(x)\}\,dx'$$
$$+O\left[\frac{\{F_1(x')-F_1(x)\}R_0 l}{L^2}\right]+O\left[\frac{\{F_1(x')-F_1(x)\}R_0 L}{l^2}\right], \qquad (2.4)$$

where

$$E_1(x) = \tfrac{1}{2}\operatorname{arcsinh}\left(\frac{l+x}{2L}\right)+\tfrac{1}{2}\operatorname{arcsinh}\left(\frac{l-x}{2L}\right)$$
$$+\frac{l+x}{4\{(l+x)^2+4L^2\}^{\frac{1}{2}}}+\frac{l-x}{4\{l-x)^2+4L^2\}^{\frac{1}{2}}}.$$

To solve (2.4), an iterative procedure is used with

$$F_1(x) = \epsilon F_1^{(1)}(x)+\epsilon^2 F_1^{(2)}(x)+\epsilon^3 F_1^{(3)}(x)+\ldots.$$

When this is substituted into (2.4) and terms with the same powers of ϵ are equated they yield

$$F_1^{(1)} = 4\pi\mu U_1,$$
$$F_1^{(2)} = 4\pi\mu U_1\{E_1-\tfrac{1}{2}-\tfrac{1}{2}\ln(1-x^2/l^2)\},$$
$$F_1^{(3)} = 4\pi\mu U_1\{E_1-\tfrac{1}{2}-\tfrac{1}{2}\ln(1-x^2/l^2)\}^2$$
$$+\frac{1}{2}\int_{-l}^{+l}\left[\frac{1}{|x'-x|}-\frac{(x-x')^2+6L^2}{\{(x-x')^2+4L^2\}^{\frac{3}{2}}}\right]\{F_1^{(2)}(x)-F_1^{(2)}(x')\}\,dx'.$$

The total drag on the rod is found to be

$$\mathscr{F}_1 = \int_{-l}^{+l}F_1(x)\,dx$$
$$= 4\pi\mu U_1\epsilon l\left[2+\epsilon\left\{W_1-1-\frac{1}{2}\int_{-1}^{+1}\ln(1-\xi^2)\,d\xi\right\}\right.$$
$$\left.+\epsilon^2 Q_1+O(\epsilon^3)+O(\epsilon R_0/L)+O(\epsilon R_0/l)\right], \qquad (2.5)$$

where $W_1 = 2\operatorname{arcsinh}(l/L)-[1+(L/l)^2]^{\frac{1}{2}}+(L/l)$ and

$$Q_1 = \frac{1}{2}\int_0^1\left[\ln(1-\xi^2)+1-\operatorname{arcsinh}\frac{l(1+\xi)}{2L}-\operatorname{arcsinh}\frac{l(1-\xi)}{2L}\right.$$
$$\left.-\frac{1+\xi}{2\{(1+\xi)^2+(2L/l)^2\}^{\frac{1}{2}}}-\frac{1-\xi}{2\{(1-\xi)^2+(2L/l)^2\}^{\frac{1}{2}}}\right]^2 d\xi,$$

since the contribution to the total drag from the integral expression in $F_1^{(3)}$ is zero. The expression (2.5) for the drag is valid even when the rod is quite close to the wall, whereas for non-slender bodies the mirror-image technique has so far only produced results that are valid in the far field.

If (2.5) is compared with the corresponding result for a rod falling in unbounded fluid [see Batchelor (1970), equation (8.12)] it is observed that the dominant part of the drag due to the presence of the wall is $4\pi\mu U_1 l W_1 \epsilon^2$. As $l/L \to 0$,

$$W_1 = 3l/2L + O(l/L)^3$$

so

$$\mathscr{F}_1 = 4\pi\mu U_1 \epsilon l \left[2 + \epsilon\left\{-1 - \frac{1}{2}\int_{-1}^{+1} \ln(1-\xi^2)\,d\xi + \frac{3l}{2L} + O\left(\frac{l}{L}\right)^3\right\} + O\left(\frac{\epsilon R_0}{l}\right) + O(\epsilon^2)\right].$$

This last result agrees with that deduced from Brenner (1962) for any body falling parallel to a single plane wall and at a distance from it large compared with the dimensions of the body.

A drag coefficient C_1 is obtained from (2.5) by dividing through by $4\pi\mu U_1 l$, which can be thought of as the drag on a sphere falling with the rod's speed and whose radius is one third of the length of the rod. Thus

$$\begin{aligned} C_1 &\equiv \mathscr{F}_1/4\pi\mu U_1 l \\ &= 2\epsilon + \epsilon^2\left\{W_1 - 1 - \frac{1}{2}\int_{-1}^{+1} \ln(1-\xi^2)\,d\xi\right\} + \epsilon^3 Q_1 + O(\epsilon^4) + O\left(\frac{\epsilon^2 R_0}{L}\right) + O\left(\frac{\epsilon^2 R_0}{l}\right). \end{aligned} \tag{2.6}$$

Since the drag on a body falling at terminal speed is balanced by its apparent weight, this drag coefficient can also be calculated in the form

$$C_{1E} = R_0^2(\rho - \rho')\,g/2\mu U_1, \tag{2.7}$$

where ρ is the density of the rod and ρ' is the density of the fluid. This value C_{1E} can be determined from experimental observations and will be compared with the value C_1 given in (2.6) which results from the theory.

Expansions of u and w on the basis of slender-body theory can now be obtained on the rod's surface by using (2.1) and (2.3) with the above solution for F_1. But $u = 0$ and $w = 0$ on the rod's surface, and to enable these boundary conditions to be satisfied the correct leading higher-order Stokeslet singularities and potential flow singularities could now be obtained if they were required.

Some interesting results occur for a slender rod falling parallel to a vertical plane wall but with orientations different from that considered in this section. If the rod falls with a vertical orientation or with its axis perpendicular to the wall the no-slip condition in the streamwise direction again yields slender-body approximations for the unknown Stokeslet strength distributions, but it is not possible to choose higher-order Stokeslet singularities or potential flow singularities that will give zero velocity components on the rod in the other two directions. In both these cases, the velocity distributions on the surface of the rod predict that the rod cannot maintain its specified orientation. The rod with the vertical orientation begins to tilt such that its leading edge moves away from the wall, while the rod normal to the wall tilts in such a way that the end further from the wall falls faster than the near end. Such predictions have been confirmed by experiment and indicate why the particular orientation of the rod considered in this section is the most useful one for experiments that involve a rod near a single wall.

2.2. *Horizontal orientation, two parallel plane walls*

For a rod in a horizontal orientation moving transversely with velocity U_2 parallel to and midway between two fixed parallel vertical plane walls, the same rectangular co-ordinate system is used as in §2.1 with the walls at $z = \pm L$ (see figure 1). Consider a line distribution of Stokeslets with strengths $(0, F_2(x), 0)$ covering the portion $-l < x < +l$, $y = 0, z = 0$ of the cylinder's axis, then for flows involving an unbounded fluid in which inertia forces are neglected the perturbation velocity components at any point (x, y, z) may be represented by (u_0, v_0, w_0) of §2.1 with F_2 replacing F_1.

As mentioned earlier the mirror-image technique does not produce useful results for the double-wall situation, mainly because the boundary conditions on the two walls have to be applied one after the other in a continuous iterative process, which leads after some lengthy calculations to a divergent series expression for the drag. On the other hand, Faxen (1923) (see also Happel & Brenner 1965, pp. 323–324) considered the problem of a sphere falling between two parallel walls and discussed a technique which enabled him to apply the no-slip condition on both walls at the same point of procedure.

The first step in adapting this procedure to the present problem leads to the identity

$$\frac{1}{r_0} \equiv \frac{1}{2\pi}\int_{-\infty}^{+\infty}\int_{-\infty}^{+\infty}\frac{1}{k}\exp\left[i(\alpha x - \alpha x' + \beta y) - k|z|\right]d\alpha\, d\beta,$$

where $k = (\alpha^2+\beta^2)^{\frac{1}{2}}$. This double integral and its partial derivatives with respect to x, y and z may be used to express the unbounded solution (u_0, v_0, w_0) entirely in terms of the Cartesian co-ordinate system; thus

$$v_0 = \frac{1}{16\pi^2\mu}\int_{-l}^{+l}\int_{-\infty}^{+\infty}\int_{-\infty}^{+\infty}\left\{\frac{2}{k} - \frac{\beta^2(1+k|z|)}{k^3}\right\}\exp\left[i(\alpha x - \alpha x' + \beta y) - k|z|\right] \times F_2(x')\, d\alpha\, d\beta\, dx',$$

while u_0 and w_0 are given by similar expressions with the term in braces replaced by $-\alpha\beta(1+k|z|)/k^3$ and $-i\beta z/k$ respectively.

Faxen established that one general solution of the creeping-motion equations is

$$u^* = \frac{1}{2\pi}\int_{-\infty}^{+\infty}\int_{-\infty}^{+\infty} i\alpha\left\{\frac{i\beta(1+kz)\,g_1^*}{k^3} + \frac{g_2^*}{k} - \frac{i\beta z g_3^*}{k}\right\}\exp\left[i(\alpha x + \beta y) - kz\right]d\alpha\, d\beta,$$

$$v^* = \frac{1}{2\pi}\int_{-\infty}^{+\infty}\int_{-\infty}^{+\infty}\left\{\frac{2g_1^*}{k} - \frac{\beta^2(1+kz)\,g_1^*}{k^3} + \frac{i\beta g_2^*}{k} + \frac{\beta^2 z g_3^*}{k}\right\}\exp\left[i(\alpha x + \beta y) - kz\right]d\alpha\, d\beta,$$

$$w^* = \frac{1}{2\pi}\int_{-\infty}^{+\infty}\int_{-\infty}^{+\infty}\left\{-\frac{i\beta z g_1^*}{k} - g_2^* + \frac{i\beta(1+kz)\,g_3^*}{k}\right\}\exp\left[i(\alpha x + \beta y) - kz\right]d\alpha\, d\beta,$$

where the g_j^* $(j = 1, 2, 3)$ may be arbitrary functions of α and β. He also gave another general solution (u^{**}, v^{**}, w^{**}) which can be obtained by replacing k by $-k$ and g_j^* by g_j^{**} everywhere in the expressions for (u^*, v^*, w^*).

The full perturbation velocity solution (u, v, w) is expressed at this stage as the sum of the solutions (u_0, v_0, w_0), (u^*, v^*, w^*) and (u^{**}, v^{**}, w^{**}); and from this the boundary conditions

$$u_0 + u^* + u^{**} = 0, \quad v_0 + v^* + v^{**} = 0 \quad \text{and} \quad w_0 + w^* + w^{**} = 0$$

on the walls $z = \pm L$ yield six linear equations for the unknown functions g_j^* and g_j^{**}. Thus Faxen's technique enables the no-slip condition to be applied on both walls simultaneously. The solution set of these equations is

$$g_1^* = -g_1^{**} = \frac{-1}{8\pi\mu(e^{2kL}+1)}\int_{-l}^{+l} F_2(x')\,e^{-i\alpha x'}\,dx',$$

$$g_2^* = \quad g_2^{**} = \frac{i\beta L(e^{2kL}-kLe^{2kL}-1-kL)}{4\pi\mu k(e^{2kL}+1)\,(e^{-2kL}+4kL-e^{2kL})}\int_{-l}^{+l} F_2(x')\,e^{-i\alpha x'}\,dx',$$

$$g_3^* = -g_3^{**} = \frac{L(e^{2kL}-1)}{4\pi\mu(e^{2kL}+1)\,(e^{-2kL}+4kL-e^{2kL})}\int_{-l}^{+l} F_2(x')\,e^{-i\alpha x'}\,dx'.$$

Thus

$$v = v_0 + \frac{1}{16\pi^2\mu}\int_{-\infty}^{+\infty}\int_{-\infty}^{+\infty}\int_{-l}^{+l} \exp\left[i(\alpha x - \alpha x' + \beta y)\right] F_2(x')\,G(\alpha,\beta,z)\,dx'\,d\alpha\,d\beta, \tag{2.8}$$

where $G(\alpha,\beta,z)$ need not be written down explicitly because the particular result required for this paper is

$$G(\alpha,\beta,0) = \frac{1}{(e^{2kL}+1)}\left\{\frac{4}{k} + \frac{4\beta^2 L(e^{2kL}-kL\,e^{2kL}-1-kL)}{k^2(e^{-2kL}+4kL-e^{2kL})} - \frac{2\beta^2}{k^3}\right\}.$$

Two corresponding expressions for the other velocity components u and w could be given, but as in the previous section an approximation for the unknown strengths F_2 can be obtained via slender-body theory using only the streamwise velocity component.

Therefore, from (2.8), the boundary condition $v = U_2$ at any point (x_s, y_s, z_s) of the rod's curved surface yields

$$\begin{aligned}
8\pi\mu U_2 = {} & F_2(x_s)\int_{-l}^{+l}\left(\frac{1}{r_{0s}} + \frac{x_s^2}{r_{0s}^3}\right)dx' \\
& + \frac{F_2(x_s)}{2\pi}\int_{-\infty}^{+\infty}\int_{-\infty}^{+\infty}\int_{-l}^{+l} \exp\left[i(\alpha x_s - \alpha x' + \beta y_s)\right] G(\alpha,\beta,z_s)\,dx'\,d\alpha\,d\beta \\
& + \int_{-l}^{+l}\left(\frac{1}{r_{0s}} + \frac{x_s^2}{r_{0s}^3}\right)\{F_2(x') - F_2(x_s)\}\,dx' \\
& + \frac{1}{2\pi}\int_{-\infty}^{+\infty}\int_{-\infty}^{+\infty}\int_{-l}^{+l} \exp\left[i(\alpha x_s - \alpha x' + \beta y_s)\right]\{F_2(x') - F_2(x_s)\}\,G(\alpha,\beta,z_s)\,dx'\,d\alpha\,d\beta.
\end{aligned}$$

With $y_s = R_0\cos\theta$ and $z_s = R_0\sin\theta$, these four integrals can each be expanded for small R_0/l, where it is assumed that R_0/L is not larger than R_0/l. (In the experiments performed $L = 15{\cdot}1$ cm while l ranged from $1{\cdot}25$ to $4{\cdot}45$ cm.)

A procedure similar to that discussed in §2.1 leads to the following integral equation for F_2 (again dropping the s subscript):

$$\begin{aligned}
4\pi\mu U_2 = {} & F_2(x)\left[\frac{1}{\epsilon} + \tfrac{1}{2} + \tfrac{1}{2}\ln\left(1 - \frac{x^2}{l^2}\right)\right. \\
& \left. - \frac{1}{2\pi}\int_{-\infty}^{+\infty}\int_{-\infty}^{+\infty} e^{i\alpha x}\,G(\alpha,\beta,0)\,\frac{\sin\alpha l}{\alpha}\,d\alpha\,d\beta + O\left(\frac{R_0}{l}\right)\right] \\
& - \frac{1}{4\pi}\int_{-\infty}^{+\infty}\int_{-\infty}^{+\infty}\int_{-l}^{+l} e^{i\alpha(x-x')}\{F_2(x') - F_2(x)\}\,G(\alpha,\beta,0)\,dx'\,d\alpha\,d\beta \\
& + \frac{1}{2}\int_{-l}^{+l}\frac{F_2(x') - F_2(x)}{|x-x'|}\,dx' + o\left(\frac{R_0 F_2}{l}\right).
\end{aligned} \tag{2.9}$$

Using the same iterative procedure as before, the approximate solution of (2.9) is seen to be

$$F_2(x) = 4\pi\mu U_2[\epsilon + \epsilon^2\{-\tfrac{1}{2} - \tfrac{1}{2}\ln(1-x^2/l^2) + E_2(x)\} + O(\epsilon^3) + O\{\epsilon^2 R_0/l\}],$$

where

$$E_2(x) = \frac{1}{2\pi}\int_{-\infty}^{+\infty}\int_{-\infty}^{+\infty} e^{i\alpha x}\, G(\alpha,\beta,0)\frac{\sin\alpha l}{\alpha}\, d\alpha\, d\beta.$$

The total drag on the rod is thus given by

$$\begin{aligned}\mathscr{F}_2 &= \int_{-l}^{+l} F_2(x)\, dx \\ &= 4\pi\mu U_2 \epsilon l\left[2 + \epsilon\left\{W_2 - 1 - \frac{1}{2}\int_{-1}^{+1}\ln(1-\xi^2)\, d\xi\right\} + O(\epsilon^2) + O\left(\frac{\epsilon R_0}{l}\right)\right], \quad (2.10)\end{aligned}$$

where

$$W_2 = \frac{L}{\pi l}\int_0^{2\pi}\int_0^{\infty}\frac{\sin^2(Kl\cos\phi/L)}{K^2\cos^2\phi}\, H(K,\phi)\, dK\, d\phi,$$

with $\alpha = k\cos\phi$, $\beta = k\sin\phi$, $K = kL$ and $H(K,\phi)$ defined by

$$(e^{2K}+1)H = 4 - \sin^2\phi\left\{2 - \frac{4K(e^{2K} - Ke^{2K} - 1 - K)}{(e^{-2K} + 4K - e^{2K})}\right\}.$$

Again, comparison with the result for unbounded fluid shows that the dominant part of the drag due to the wall's presence is $4\pi\mu U_2 l W_2 \epsilon^2$. As $l/L \to 0$,

$$W_2 = \frac{l}{L}\int_0^{\infty}\frac{1}{(e^{2K}+1)}\left\{6 + \frac{4K(e^{2K} - Ke^{2K} - 1 - K)}{(e^{-2K} + 4K - e^{2K})}\right\} dK + O\left(\frac{l}{L}\right)^3;$$

numerical evaluation of the integral gives

$$W_2 = 2{\cdot}677 l/L + O(l/L)^3,$$

a result which is the same as would be obtained from Brenner's formula (1962) for a body falling midway between two parallel walls and at a distance from them which is large compared with a typical length measurement of the body.

From (2.10) the drag coefficient is

$$\begin{aligned}C_2 &\equiv \mathscr{F}_2/4\pi\mu U_2 l \\ &= 2\epsilon + \epsilon^2\left\{W_2 - 1 - \frac{1}{2}\int_{-1}^{+1}\ln(1-\xi^2)\, d\xi\right\} + O(\epsilon^3) + O\left(\frac{\epsilon^2 R_0}{l}\right) \quad (2.11)\end{aligned}$$

as $\epsilon \to 0$, which will be compared in the latter part of the paper with the experimental drag coefficient

$$C_{2E} = R_0^2(\rho - \rho')\, g/2\mu U_2 \quad (2.12)$$

based on an experimentally measured U_2.

2.3. *Vertical orientation, two parallel plane walls*

Consider a rod in a vertical orientation moving longitudinally with velocity U_3 parallel to and midway between the same two walls of the problem in §2.2. The methods of that section can then be applied to a line distribution of Stokeslets that are directed along the segment of the rod's axis that lies inside the cylinder.

This leads to a slender-body approximation for the Stokes-flow drag on the rod given by

$$\mathscr{F}_3 = 2\pi\mu U_3\, \epsilon l\left[2+\epsilon\left\{W_3+1-\frac{1}{2}\int_{-1}^{+1}\ln(1-\xi^2)\,d\xi\right\}+O(\epsilon^2)+O\left(\frac{\epsilon R_0}{l}\right)\right], \quad (2.13)$$

where

$$W_3 = \frac{L}{2\pi l}\int_0^{2\pi}\int_0^{\infty}\frac{\sin^2(Kl\sin\phi/L)}{K^2\sin^2\phi}\,H(K,\phi)\,dK\,d\phi;$$

the form for $\mathscr{F}_3$ being similar to (2.10) except for an overall factor of $\frac{1}{2}$ and one sign change in the terms of $O(\epsilon^2)$. The dominant part of the drag due to the wall effect is $2\pi\mu U_3 l W_3 \epsilon^2$, and as $l/L \to 0$

$$W_3 = 1{\cdot}339 l/L + O(l/L)^3,$$

which is again consistent with Brenner's (1962) results.

As $\epsilon \to 0$ the drag coefficient C_3 is defined by

$$\begin{aligned} C_3 &= \mathscr{F}_3/4\pi\mu U_3 l \\ &= \frac{1}{2}\left[2\epsilon+\epsilon^2\left\{W_3+1-\frac{1}{2}\int_{-1}^{+1}\ln(1-\xi^2)\,d\xi\right\}+O(\epsilon^3)+O\left(\frac{\epsilon^2 R_0}{l}\right)\right] \end{aligned} \quad (2.14)$$

and this will be compared with the experimental drag coefficient

$$C_{3E} = R_0^2(\rho-\rho')\,g/2\mu U_3, \quad (2.15)$$

based on an experimental value for U_3.

3. Experimental procedure

A steel-framed tank with a rectangular base 104 cm by 30 cm and four plane non-distorted glass walls of height 59 cm was placed in a controlled-temperature room and filled to a depth of 56 cm with liquid glucose.

Welding rods and wires, cut and machined into various lengths, proved suitable circular cylinders for the experiments, as did the axles of a Meccano set available commercially. From the measurements of each cylinder's mass, length and diameter, its density ρ was calculated and is presented in table 1 together with the length-to-thickness ratios (to give some idea of slenderness) and the values of the thickness-to-length parameter ϵ.

Note how slowly the parameter ϵ varies: while the length-to-thickness ratio increases from 10 to 100, ϵ changes only from 0·34 to 0·19 and to achieve a value of 0·1 for ϵ would require $l/R_0 = 11\,000$, which is impractical for experiments of this nature. The theory involves expansions in powers of ϵ and so will give best results when ϵ is small. The values of ϵ which had to be used are not particularly small and so provide a fairly severe test of the theory, but since they refer to slender bodies with practical length-to-thickness ratios a consistently large difference between the theoretical and the experimental results would indicate that slender-body theory remains a theory only.

In the first of three series of experiments nine different rods were used. Each rod fell in a horizontal orientation with its axis of symmetry parallel to and at a distance 1·1 cm from a long wall, while its centre was equidistant from both short

Material	$2l$ (cm)	R_0 (cm)	l/R_0	ϵ	ρ (g/ml)
Welding rod	2·50	0·080	15·6	0·291	7·820
Welding rod	2·89	0·080	18·1	0·279	7·820
Meccano rod	2·96	0·076	19·5	0·273	7·652
Copper-coated steel rod	2·99	0·160	9·3	0·343	7·986
Piano wire	3·14	0·050	31·4	0·242	9·895
Welding rod	3·74	0·080	23·4	0·260	7·820
Thin wire	3·98	0·036	55·3	0·213	7·467
Welding rod	4·37	0·080	27·3	0·250	7·820
Wire	4·93	0·044	55·5	0·212	7·698
Welding rod	5·89	0·080	36·8	0·233	7·820
Wire	6·59	0·044	74·2	0·200	7·698
Thin wire	7·06	0·036	98·1	0·190	7·467
Welding rod	7·47	0·080	46·7	0·221	7·820
Welding rod	8·90	0·080	55·6	0·212	7·820

TABLE 1. Dimensions and characteristics of circular cylindrical rods

walls. This position and orientation was achieved by making the rod slide from a thin metal strip whose end was just below the free surface of the glucose.

The second series of experiments used twelve rods, seven of them having been used in the previous series. Again each rod fell with a horizontal orientation but the position of the fall was altered to halfway between both the long and the short walls, that is, down the centre of the tank.

An equivalent set of twelve rods was used in the final series of experiments, in which each rod fell with a vertical orientation down the centre of the tank. This orientation was obtained by releasing a dry rod down a glass tube clamped in a vertical position above the surface of the liquid.

A thermometer was suspended in the glucose for the duration of the experiments and the temperature was recorded frequently. The readings indicated that the temperature of the liquid varied inside the range for the surrounding air (20 °C–22 °C), and that these variations took place on a time scale much longer than the recorded times of fall. Preliminary experiments with spheres of various sizes established that in this temperature range the glucose behaved as a Newtonian fluid with a dynamic viscosity of approximately 50 P and a density (ρ') equal to 1·396 g/ml.

After each rod had fallen to the bottom of the tank a standard sphere (mass 0·032 g, radius 0·089 cm) was released at the centre of the surface and timed over a 20 cm fall. The value of μ can then be obtained from the well-known formula related to the Stokes-flow drag on a sphere in unbounded fluid, namely

$$\mu = 2a^2(\rho_s - \rho')g/9U_s,$$

where $\rho_s - \rho' = 9{\cdot}434$ g/ml with U_s, a and ρ_s representing the sphere's terminal speed, radius and density respectively. There are two possible sources of error in using this result. One is associated with a correction for the effect of the container walls and is negligible because of the size of the sphere in comparison with

its distance from the nearest wall. The other, due to inertial effects, is less than $\frac{1}{2}\%$ for the spheres used.

However in the formulae to be verified μ only occurs in the three alternative forms of the drag coefficient given by (2.7), (2.12) and (2.15), so these can now be written as

$$C_{jE} = 9R_0^2(\rho-\rho')\,U_s/4a^2(\rho_s-\rho')\,U_j \quad (j = 1,2,3). \tag{3.1}$$

The two series of experiments down the centre of the tank were conducted together. A complete run of the experimental procedure consisted of successive falls of (i) a rod in a horizontal orientation, (ii) a standard sphere, (iii) an equivalent rod in a vertical orientation and (iv) a standard sphere. When the sphere times agreed the experimental run was considered to have been performed at a constant viscosity, and then the rod times could be used to give a value of the ratio of the longitudinal and transverse speeds of fall for that particular rod.

Using a Pye laboratory clock in conjunction with a cathetometer, at least three times of fall were recorded for each rod from a level 8 cm below the surface of the glucose to a level 8 cm above the bottom of the tank, this being done in stages of 5 or 10 cm depending on the slowness of the rod's fall. The averages of these times over the central 20 cm of fall appear in the tables of the next section.

4. Comparison and discussion

The results for each series of experiments are tabulated in tables 2–4, each of which contains six columns. The first column contains the rod length ($2l$) for identification purposes. The next two columns record the falling time of a standard sphere (t_s) and the average falling time of each rod ($t_j; j = 1,2,3$); a simple quotient then yields the ratio U_s/U_j of the sphere's speed to the rod's speed which appears in the fourth column. Column five contains the value of the experimental drag coefficient for each rod calculated from equation (3.1), while the final column gives the theoretical value of the drag coefficient for each rod calculated for table 2 from equation (2.6), for table 3 from equation (2.11) and for table 4 from equation (2.14).

For the two series of experiments involving the fall of horizontal rods the comparison of drag coefficients shows that the theoretical value is at most 12% less than the experimental value. In particular for a horizontal rod falling down the centre of the tank, ten of the rods had theoretical and experimental results agreeing to within 5% or better. On the other hand, that series of experiments concerned with the fall of vertical rods down the centre resulted in a difference between theory and experiment ranging from 12 to 24%.

A feature of each table is that the theoretical analysis predicts values that are less than the experimental results in most cases. This is not surprising since the theoretical formulae tested are based on the presence of either one or two walls only, and do not take account of the remaining walls. However, it appears to happen often in Stokes-flow wall-effect theory that the drag caused by two walls is slightly less than the cumulative drags due to each wall separately (see Happel & Brenner 1965, pp. 327–328). Assuming this happens here also, an upper bound can be obtained in each case for the extra drag produced by these

$2l$ (cm)	t_s (s)	t_1 (s)	U_s/U_1	Drag coefficients C_1 Observation	Theory
2·50	71·5	40·0	0·559	0·692	0·697
2·96	71·0	44·5	0·627	0·682	0·668
2·99	72·0	13·0	0·181	0·920	0·893
3·14	72·0	72·0	1·000	0·640	0·583
3·98	79·0	191·5	2·424	0·574	0·522
4·37	72·0	41·5	0·576	0·713	0·649
4·93	72·0	103·0	1·431	0·535	0·540
6·59	82·0	127·0	1·549	0·579	0·528
7·47	73·0	37·0	0·507	0·627	0·617

TABLE 2. Comparison of experimental and theoretical drag coefficients for a horizontal rod falling with its axis parallel to and at a distance 1·1 cm from a single plane vertical wall

$2l$ (cm)	t_s (s)	t_2 (s)	U_s/U_2	Drag coefficients C_2 Observation	Theory
2·50	72·0	33·5	0·465	0·576	0·567
2·89	71·5	33·0	0·462	0·571	0·547
2·96	67·0	34·5	0·515	0·560	0·537
3·14	67·0	56·0	0·836	0·535	0·477
3·74	69·0	30·0	0·435	0·538	0·517
4·37	69·0	29·0	0·420	0·520	0·500
4·93	70·0	82·5	1·179	0·441	0·427
5·89	70·5	29·0	0·411	0·509	0·472
6·59	74·0	82·0	1·108	0·414	0·408
7·06	68·5	112·0	1·635	0·387	0·387
7·47	68·5	26·0	0·380	0·470	0·454
8·90	68·0	25·5	0·375	0·464	0·442

TABLE 3. Horizontal rod falling with its axis parallel to and midway between two parallel vertical walls which are 30·2 cm apart

$2l$ (cm)	t_s (s)	t_3 (s)	U_s/U_3	Drag coefficients C_3 Observation	Theory
2·50	72·0	24·5	0·340	0·421	0·363
2·89	71·5	24·0	0·336	0·415	0·346
2·96	67·0	24·0	0·358	0·390	0·338
3·14	67·0	38·0	0·567	0·363	0·293
3·74	69·0	20·0	0·290	0·359	0·320
4·37	69·0	19·5	0·283	0·350	0·307
4·93	70·0	57·0	0·814	0·305	0·254
5·89	70·5	19·5	0·277	0·343	0·283
6·59	74·0	54·5	0·737	0·275	0·238
7·06	68·5	76·0	1·110	0·263	0·224
7·47	68·5	17·5	0·256	0·316	0·268
8·90	68·0	17·0	0·250	0·310	0·257

TABLE 4. Vertical rod falling with its axis parallel to and midway between two parallel vertical walls which are 30·2 cm apart

extraneous walls. These appear to be less than 4 % for the first series of experiments and less than 3 % for the other two series.

Other sources of extra drag are the free surface of the glucose and the bottom of the tank. Although difficult to estimate, it seems plausible to assume that they have a small effect over the central 20 cm of the measurement. This assumption is supported by the consistency of the time of fall through each 5 or 10 cm stage.

Apart from these positive increments to the theoretical drag coefficients there are error terms of unknown sign associated with formulae (2.6), (2.11) and (2.14). The values quoted in table 2 for the theoretical coefficient C_1 include the numerical evaluation of $\epsilon^3 Q_1$, and the expansion error terms are of order 0·5–1·5 % (for ϵ^4 terms) and 0·5–2 % (for $\epsilon^2 R_0/L$ terms).

Terms of order ϵ^3 are not explicitly included in the theoretical expressions for C_2 and C_3 as they are difficult to evaluate numerically. The expansion error terms in these two results are then of order 2–5 % (for ϵ^3 terms) and 0·2–2 % (for $\epsilon^2 R_0/l$ terms).

The maximum percentage error for the experimental drag coefficients C_{jE} is 12 %, obtained from (3.1) through probable measurement errors of 1 % in R_0, 1 % in a, 2 % in $\rho_s - \rho'$, 2 % in $\rho - \rho'$, 2 % in U_s and 2 % in U_j.

Now the Reynolds number of the flow associated with a standard sphere is of $O(10^{-3})$, while that for the flow due to the falling rods ranges from 0·02 to 0·2 (based on rod lengths) or from 0·1 to 0·4 (based on the half-distance L between the two walls). Therefore, the comparison of the experimental results with those obtained from a Stokes-flow analysis seems reasonably justified.

The experimental and theoretical drag coefficients are in good agreement for rods falling with a horizontal orientation, but the error bounds cannot account for the discrepancy in the results for rods falling with a vertical orientation. Rosen (1972) noted a similar discrepancy when comparing experimental and numerical results for non-slender bodies of other shapes falling longitudinally. Perhaps inertial effects or the top and bottom boundaries of the glucose have a greater influence on the longitudinal-fall experiments than on the transverse-fall experiments. Alternatively, limitations of the theory in approximately replacing the slender body by a line distribution of Stokeslets may possibly cause errors near the ends of the rod that are more significant for longitudinal flow than for transverse flow over the range of ϵ tested.

The second and third series of experiments were designed to produce experimental values for the ratio (U_3/U_2) of the speed of fall of a rod in a vertical orientation to its speed of fall in a horizontal orientation over different values of ϵ. Twelve values of this ratio between 1·36 and 1·51 can be obtained from tables 3 and 4, and – despite the shortcomings of the third series of experiments – these indirectly support the now well-established theoretical fact (Weinberger 1972) that the ratio in an unbounded fluid approaches the limit 2 from below as $\epsilon \to 0$. It was recent assertions concerning the value of this ratio which led to the current upsurge of interest in slender-body theory.

The author acknowledges that the initial stimulus for this work came from discussions with Professor G. K. Batchelor. Preliminary experiments were carried

out in conjunction with Mr T. Parkes, also of the Mathematics Department at Duntroon, and the author is grateful for his help in this developmental part of the work. Appreciation is also expressed to the Chemistry Department at Duntroon for the use of the controlled-temperature room and other equipment, to Mr C. W. Thomas for his efforts with the diagram, and to the referees for helpful comments.

REFERENCES

BATCHELOR, G. K. 1970 *J. Fluid Mech.* **44**, 419.

BLAKE, J. R. 1971 *Proc. Camb. Phil. Soc.* **70**, 303.

BRENNER, H. 1962 *J. Fluid Mech.* **12**, 35.

CLARKE, N. S. 1972 *J. Fluid Mech.* **52**, 781.

COX, R. G. 1970 *J. Fluid Mech.* **44**, 791.

COX, R. G. 1971 *J. Fluid Mech.* **45**, 625.

FAXEN, H. 1923 *Arkiv. Mat. Astr. Fys.* **17**, no. 27.

HAPPEL, J. & BRENNER, H. 1965 *Low Reynolds Number Hydrodynamics.* Prentice-Hall.

JONES, A. M. & KNUDSEN, J. G. 1961 *A.I.Ch.E. J.* **7**, 20.

LORENTZ, H. A. 1896 *Zittingsverlag. Akad. v. Wert.* **5**, 168.

ROSEN, A. L. 1972 *J. Inst. Math. Applics.* **9**, 280.

TAYLOR, G. I. 1969 *Problems of Hydrodynamics and Continuum Mechanics*, p. 718. S.I.A.M. Publications.

TILLETT, J. P. K. 1970 *J. Fluid Mech.* **44**, 401.

TUCK, E. O. 1964 *J. Fluid Mech.* **18**, 619.

TUCK, E. O. 1968 *Proc. 3rd Austr. Conf. on Hydraulics & Fluid Mech.* p. 29. Sydney: Inst. Engrs Austr.

WEINBERGER, H. F. 1972 *J. Fluid Mech.* **52**, 321.

WHITE, C. M. 1946 *Proc. Roy. Soc.* A **186**, 472.